# Analytical prediction of active-layer thaw and subsidence under seasonal thermal forcing: application to Svalbard permafrost

Land McCormick[1,2,*], and Dina Schmidt[2,3]
[1] Gdańsk University of Technology, 80-233 Gdańsk, Poland
[2] Aarhus University, Aarhus, Denmark
[3] School of Biological, Earth and Environmental Sciences, University College Cork, Cork, Ireland
[*]Corresponding to: land.mccormick@gou.edu.pl

## Abstract

Seasonal thaw of the active layer and the resulting ground subsidence strongly influence Arctic hydrology, soil-carbon release, and the stability of northern infrastructure. Lunardini (1987) derived an exact similarity solution for one-dimensional thaw in frozen soil that consolidates as it thaws. Although physically elegant, the solution has remained difficult to use in practice: usable limiting formulas are lacking, parameter sensitivities remain unquantified, and performance under transient seasonal forcing has not been independently tested. Its field-scale value for active-layer and thaw-settlement prediction therefore remains largely unresolved. Here we revisit Lunardini's solution with these needs in mind. We derive closed-form small- and large-Stefan-number approximations for the thaw parameter, with errors of about 2% in the small-Stefan permafrost regime and about 1.3% in the large-Stefan regime. We then quantify dimensionless sensitivity coefficients and show that the thaw parameter responds sub-proportionally to all major inputs, with the largest controls coming from the Stefan number and the degree of initial subcooling. An independent enthalpy finite-difference model reproduces the exact solution with a mean error of 2.5%, providing a check on the implementation and a tool for transient forcing. When the similarity solution is applied to a season-mean surface temperature, it overpredicts the end-of-season active-layer thickness by roughly 8% and advances the thaw trajectory by about 2 weeks. In an illustrative Svalbard application at the Calypsostranda CALM site in Bellsund, using representative seasonal forcing and independently specified fine-soil properties, the model predicts an active-layer thickness close to the reported historical mean and a drained kinematic thaw-settlement estimate of about 5.5 cm. These results turn an exact but underused analytical solution into a practical tool for rapid active-layer and thaw-settlement estimates, while also defining when a transient numerical model is still needed.

**Keywords**: permafrost; active-layer thickness; thaw consolidation; Stefan problem; Svalbard

Date: 2026, 27 June

# 1. Introduction

Permafrost, defined as ground that remains at or below 0 °C for at least two consecutive years, underlies roughly one quarter of the exposed land surface of the Northern Hemisphere (Obu et al., 2019). It is now warming rapidly and, in many regions, degrading as climate warming intensifies. Arctic air temperatures are now increasing nearly four times faster than the global mean (Rantanen et al., 2022), and borehole records show that permafrost temperatures near the depth of zero annual amplitude increased by 0.29 ± 0.12 °C between 2007 and 2016, with the strongest warming in cold continuous permafrost (Biskaborn et al., 2019). More recent assessments confirm continued ground warming and widespread thickening of the active layer (Smith et al., 2022). Similar changes are being reported not only in Arctic lowlands, but also in high-mountain permafrost regions such as the Qinghai–Tibet Plateau, the largest high-elevation permafrost region on Earth, where continued warming is expected to deepen active layers through the present century (Peng et al., 2023).

The active layer (the near-surface soil that thaws each summer and refreezes in winter) is central to permafrost landscapes. It controls surface energy and water exchange, defines the seasonal depth available for groundwater flow and biogeochemical activity, and helps determine the bearing capacity of frozen ground (Kurylyk, 2019). Its thickness is therefore one of the most widely monitored indicators of permafrost change (Brown et al., 2000). When the active layer deepens, previously frozen organic matter becomes available for microbial decomposition, strengthening a positive feedback loop that can be amplified by abrupt thaw (Turetsky et al., 2020). Thaw also reorganizes cold-region hydrology by opening new flow paths, changing streamflow seasonality, and altering groundwater storage (Walvoord and Kurylyk, 2016; Xiang and Rudolph, 2023).

In ice-rich ground, thawing has an additional consequence: the land surface subsides as pore ice and excess ice are lost. Seasonal thaw subsidence may be only a few centimetres and partly recoverable, but in ice-rich terrain it can accumulate into larger and more persistent settlement. Such movement is now routinely measured by levelling, GPS, and satellite radar (Liu et al., 2010; Shiklomanov et al., 2013; Streletskiy et al., 2017). The engineering implications are substantial. Thaw settlement damages foundations, roads, pipelines, and other infrastructure, and the associated costs are expected to rise as permafrost continues to degrade (Hjort et al., 2022; Ran et al., 2022). Predicting both active-layer growth and the resulting settlement is therefore important for cold-region hydrology, carbon-cycle studies, and infrastructure risk assessment.

Two broad modelling approaches are commonly used. At one end are numerical thermo-hydro-mechanical models that represent coupled heat transfer, water and vapour flow, phase change, deformation, and sometimes solute transport (Huang and Rudolph, 2021, 2023; Huang et al., 2022). These models can handle soil layering, unfrozen water effects, salinity, and stress-dependent deformation, but they require many parameters and can be computationally intensive. At the other end are analytical Stefan-type solutions. These reduce the moving-boundary thaw problem to a compact equation for thaw depth and remain widely used for rapid estimates and model benchmarking (Kurylyk et al., 2014). Classical Stefan and Neumann solutions, together with extensions to layered soils, variable moisture, and conduction–advection problems (Xie and Gough, 2013; Huang and Rudolph, 2022), are attractive because they are simple and transparent. Their main limitation is that they usually assume no consolidation and no density change during thaw. Real frozen soils often do both: they expel water, lose ice volume, and densify. As a result, zero-strain Stefan solutions cannot predict thaw subsidence (Morgenstern and Nixon, 1971; Nixon, 1975).

Lunardini (1987) addressed this limitation directly. Building on the thaw-consolidation theory of Morgenstern and Nixon (1971) and earlier work on cold-region heat transfer (Lunardini, 1981, 1983, 1991; Lunardini and Varotta, 1981), he derived an exact similarity solution for one-dimensional thaw in a saturated frozen soil that consolidates as it thaws. The solution includes an expelled excess-water layer, an arbitrary ice-to-water density ratio, and convective heat transport due to the motion of the thawed soil skeleton. The full problem reduces to a single transcendental equation for a thaw parameter, γ. Once γ is known, both thaw depth and surface settlement follow. This makes the solution particularly useful: it maintains the physical link between thaw and consolidation, yet remains far simpler than a full coupled thermal-hydraulic-mechanical (THM) model.

Yet despite its elegance, Lunardini's solution has remained mostly a theoretical result. Four barriers have limited its use. First, the solution requires numerical root-finding, because no simple limiting formulas have been provided. Second, its sensitivity to uncertain inputs has not been quantified. Third, it has not been checked against an independent numerical model. Fourth, and most importantly for field applications, the similarity solution assumes that surface temperature jumps to a constant value and remains there. A real thaw season is not like this: heat is delivered gradually and unevenly. The error caused by replacing seasonal forcing with a constant mean temperature has not been measured.

This study addresses these gaps. We first derive small- and large-Stefan-number approximations that make the solution easier to use without root-finding. We then quantify the sensitivity of the thaw parameter to the main physical inputs and cross-check the exact solution against an independent enthalpy finite-difference model. Finally, we use the numerical model to quantify the error introduced by seasonal forcing and demonstrate the approach through an illustrative case study at Calypsostranda, Svalbard. The exact solution itself remains that of Lunardini (1987). We aim to make it easier to apply, to clarify its uncertainty, and to show where its practical limits lie.

## 2. The exact thaw-consolidation solution

We first restate the solution of Lunardini (1987) in the notation used below. The full derivation is given in that work. A water-saturated frozen soil (Figure 1) is initially at $T_0 < T_f$ and its surface is raised to $T_s > T_f$ at $t = 0$. Thaw expels pore water, which collects as an excess-water layer, while the ice–water density contrast opens a void; three regions result (excess water, thawed consolidated soil, frozen soil), described in moving frames $x_1, x_2, x_3$.

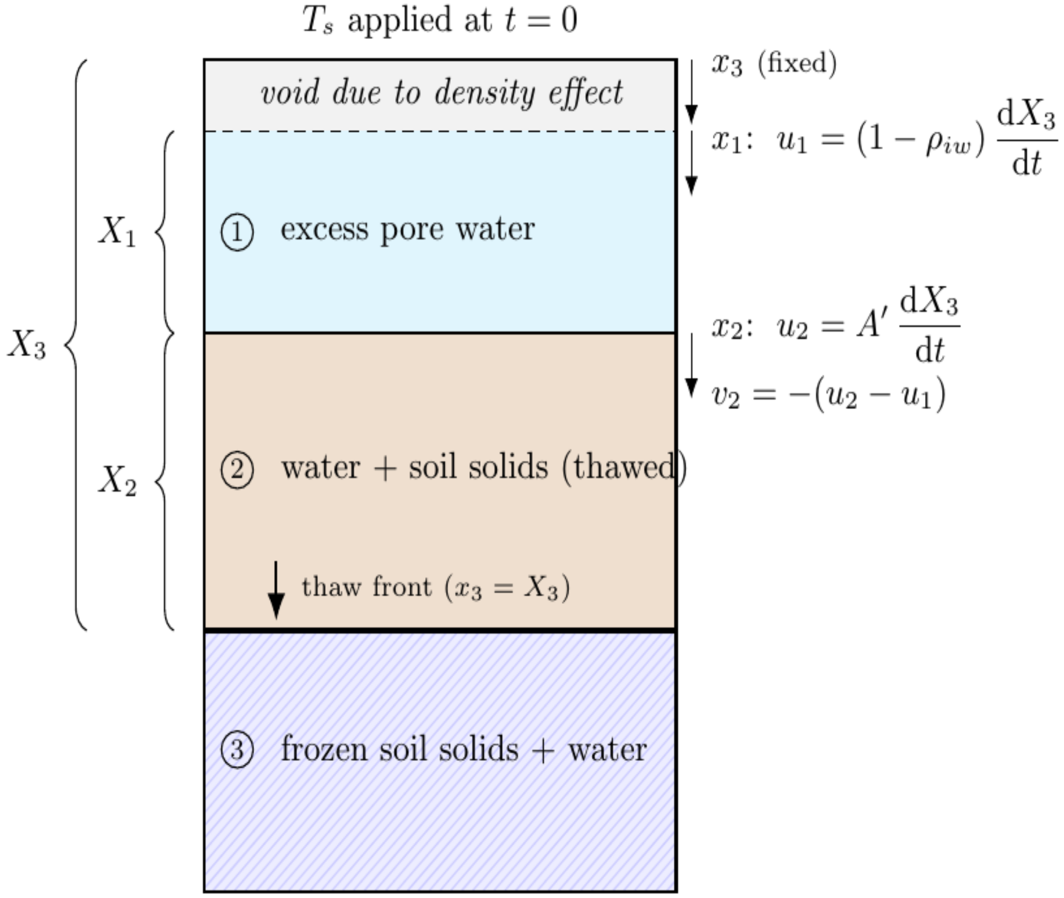

**Figure 1.** Geometry of thaw with consolidation, after Lunardini (1987). Measured downward from the original surface ($x_3 = 0$), the void occupies a thickness $(1 - \rho_{iw})X_3$, the excess water layer $X_1 = AX_3$, and the thawed soil $X_2 = (1 - A')X_3$, where $A = A' + \rho_{iw} - 1$. The thaw front is at $x_3 = X_3$.

The moving interface has velocities $u_2 = A'\,\mathrm{d}X_3/\mathrm{d}t$ and $u_1 = (1 - \rho_{iw})\,\mathrm{d}X_3/\mathrm{d}t$, where $A'$ is the thaw strain, $\rho_{iw} = \rho_i/\rho_w$, and $X_3$ is the thaw depth. The pore water moves relative to the thawed skeleton at $v_2 = -A\,\mathrm{d}X_3/\mathrm{d}t$, introducing a convective term in the thawed-zone energy equation. Conduction holds in the water and frozen layers, with continuity of temperature and flux at the interior interfaces and a Stefan condition at the thaw front. The thawed-zone temperature field has a similar form

$$T_2 = A_2 + B_2\,\mathrm{erf}(x_2/2\sqrt{\alpha_2 t} + K\gamma), \qquad X_3 = 2\gamma\sqrt{\alpha_2 t}, \tag{1}$$

with the convection absorbed exactly into the shifted argument $K\gamma$, where $K = (\rho_w c_w/\rho_2 c_2)A = A/C_{21}$. The temperature fields in the water and frozen layers take the analogous error-function forms of Lunardini (1987). Imposing all conditions reduces the problem to a single transcendental equation for $\gamma$,

$$\frac{e^{-\gamma^2(K+1-A')^2}}{P_1 + P_2} - \frac{k_{32}\sqrt{\alpha_{23}}\,\phi\, e^{-\gamma^2\alpha_{23}}}{\mathrm{erfc}\left(\gamma\sqrt{\alpha_{23}}\right)} = \frac{\sqrt{\pi}\,\gamma\,\rho_{32}}{\mathrm{Ste}} \tag{2}$$

where

$$\begin{aligned} P_1 &= k_{21}\sqrt{\alpha_{12}}\, e^{\gamma^2(A^2\alpha_{21}-K^2)}\mathrm{erf}\left(A\gamma\sqrt{\alpha_{21}}\right) - \mathrm{erf}(K\gamma), \quad P_2 = \mathrm{erf}[\gamma(K+1-A')], \\ \mathrm{Ste} &= \frac{c_2}{\ell}\left(T_s - T_f\right), \qquad \phi = \frac{T_f - T_0}{T_s - T_f}. \end{aligned} \tag{3}$$

Here $k_{ij} = k_i/k_j$, $\alpha_{ij} = \alpha_i/\alpha_j$, $\rho_{32} = \rho_3/\rho_2$, Ste is the Stefan number, and $\phi$ the subcooling. When the excess water drains instantaneously, the denominator $P_1 + P_2$ is replaced by $\mathrm{erf}[\gamma(K+1-A')] - \mathrm{erf}(K\gamma)$; when $A' = 0$ and $\rho_{iw} = 1$, (2) collapses to the two-phase Neumann problem. The saturated-soil property ratios follow the closures of Lunardini and Varotta (1981), $k_{21} = (k_w/k_s)^{x_\ell - 1}$, $k_{23} = (k_w/k_i)^{x_\ell}$, $C_{23} = 1 + (C_w/C_i - 1)x_\ell$, $C_{21} = C_s/C_w + (1 - C_s/C_w)x_\ell$, with $x_\ell$ the volumetric water content. Figure 2 shows $\gamma$ over practical ranges; the thaw rate falls sharply as the conductivity of the expelled water drops relative to that of the saturated soil.

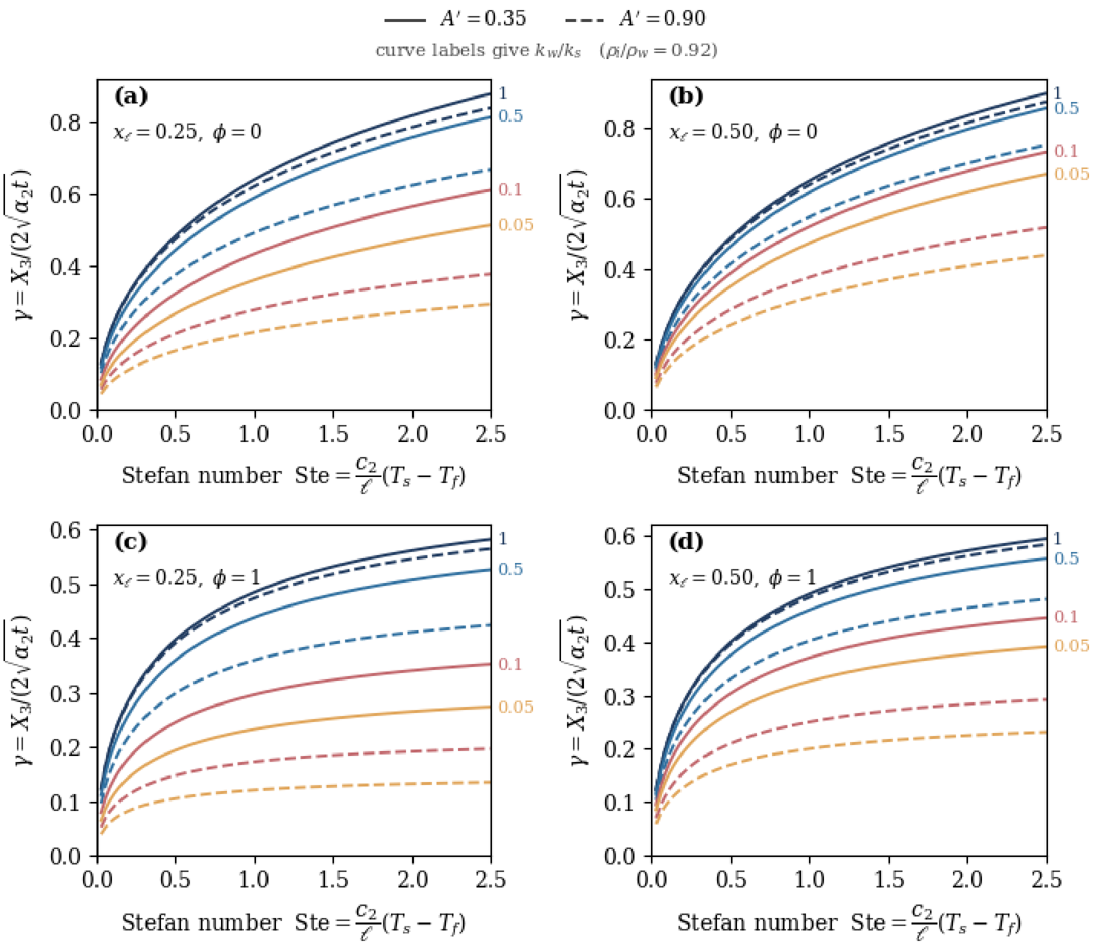

**Figure 2.** Thaw parameter $\gamma = X_3/(2\sqrt{\alpha_2 t})$ versus Stefan number, recomputed from (2) for $\rho_{iw} = 0.92$ with an excess-water layer present, for families of $k_w/k_s$ and two thaw strains ($A' = 0.35$ solid, $A' = 0.90$ dashed). Panels: (a) $x_\ell = 0.25, \phi = 0$; (b) $x_\ell = 0.50, \phi = 0$; (c) $x_\ell = 0.25, \phi = 1$; (d) $x_\ell = 0.50, \phi = 1$.

## 3. Methods

We develop three additions that make the exact solution easier to use in practice: simple limiting approximations, a sensitivity analysis, and an independent finite-difference model. The numerical model is first used to verify the exact solution under constant forcing and then to explore transient seasonal forcing, for which the similarity solution no longer holds exactly.

## 3.1 Closed-form approximations

Equation (2) generally has to be solved numerically. Two useful limits lead to simple approximations.

*Small Stefan number*. In thawing permafrost, latent heat usually dominates sensible heat, so the Stefan number is small. In this regime ( $\mathrm{Ste} \lesssim 0.2$ ), the thaw parameter ($\gamma$) is also small. Expanding the error functions in Equation (2) to first order in ($\gamma$), and keeping the leading term associated with subcooling, gives

$$\frac{2\rho_{32}D_0}{\mathrm{Ste}}\,\gamma^2 + \frac{2D_0 k_{32}\sqrt{\alpha_{23}}\,\phi}{\sqrt{\pi}}\,\gamma - 1 = 0, \qquad D_0 = k_{21}A + 1 - A', \tag{4}$$

whose positive root is the small-Stefan approximation $\gamma_\mathrm{s}$. If there is no initial subcooling ( $\phi$=0 ), it reduces to

$$\gamma_\mathrm{s} \simeq \sqrt{\frac{\mathrm{Ste}}{2\rho_{32}\,(k_{21}A+1-A')}}\,, \qquad (\phi = 0). \tag{5}$$

*Large Stefan number*. When surface superheat is large ($Ste \gg 1$), the latent-heat term becomes relatively weak and ($\gamma$) increases only slowly. In this limit, balancing the dominant exponential term with the right-hand side of Equation (2) at ($\phi = 0$) gives

$$\gamma_\mathrm{l} \simeq \sqrt{\frac{1}{C}\,\ln\frac{\mathrm{Ste}}{\sqrt{\pi}\,\rho_{32}\,\gamma_\mathrm{l}}}\,, \qquad C = (K + 1 - A')^2 + A^2\alpha_{21} - K^2, \tag{6}$$

This implicit expression converges in two or three fixed-point iterations. Figure 3 compares both approximations with the exact solution for a representative case ($A' = 0.35, x_\ell = 0.25, k_w/k_s = 0.5$). At zero subcooling, the small-Stefan formula is within 2% up to $Ste = 0.2$. Stronger subcooling increases the error, but the approximation still captures the correct scaling; for example, the error rises to about 3.7% in a small-$Ste$, high-$\phi$ estimate. The large-Stefan approximation is within about 1.3% for $Ste \geq 20$. These two limits cover the most useful parts of the parameter space and provide quick checks on numerical root-finding.

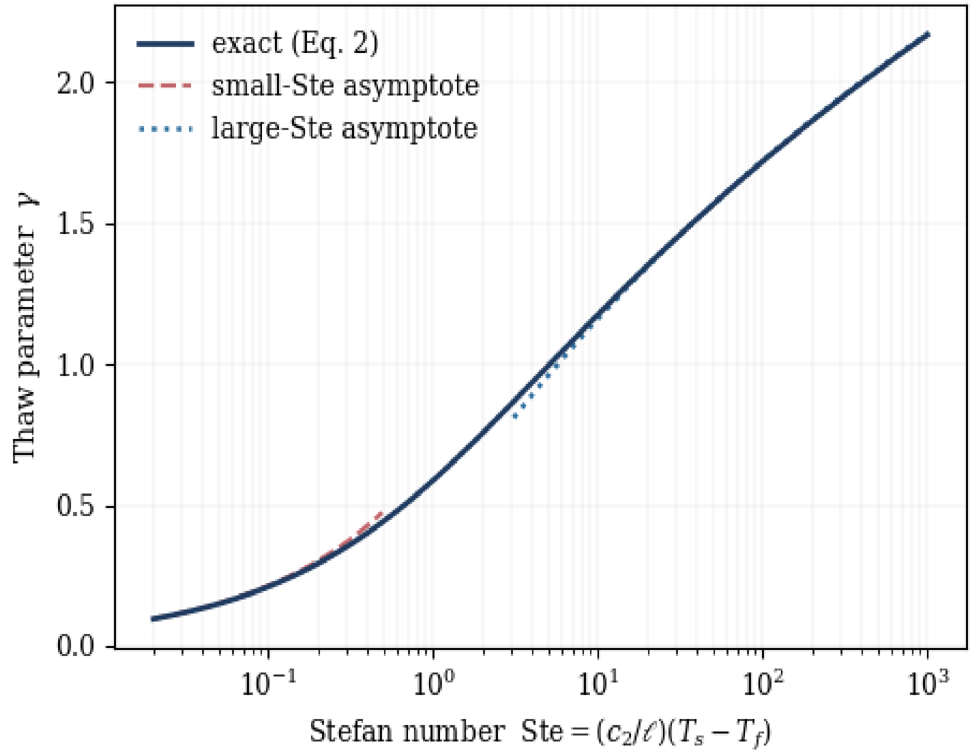

**Figure 3.** Exact thaw parameter (solid) and the small- and large-Stefan approximations (4) and (6) (dashed and dotted), each plotted over its range of validity, for $A' = 0.35$, $x_\ell = 0.25$, $k_w/k_s = 0.5$, $\phi = 0$.

### 3.2 Sensitivity and uncertainty

To assess how uncertainty in the inputs affects the thaw prediction, we write Equation (2) as $G(\gamma, \mathbf{p}) = 0$, where (p) denotes any input parameter. The implicit-function theorem gives the response of the thaw parameter to any input $p$ as $\partial\gamma/\partial p = -(\partial G/\partial p)/(\partial G/\partial\gamma)$. We report the dimensionless elasticity $E_p = (p/\gamma)\,\partial\gamma/\partial p$, which states the percentage change in $\gamma$ per percentage change in $p$ and so allows direct comparison across parameters of different units. Elasticities were evaluated at a representative baseline ($\mathrm{Ste} = 1$, $\phi = 0.5$, $A' = 0.35$, $x_\ell = 0.25$, $k_w/k_s = 0.5$) and verified against central finite differences.

The results are shown in Figure 4. The thaw parameter increases with the Stefan number ($E = +0.26$) and with the water/solid conductivity ratio ($E = +0.17$), and decreases with subcooling ($E = -0.24$) and thaw strain ($E = -0.14$); the volumetric water content has only a weak local effect ($E = +0.06$). Importantly, all elasticities have magnitudes below one. Around the baseline case, input errors therefore do not amplify into larger thaw-depth errors. This is useful for field applications, where soil and thermal properties are rarely known exactly.

The local conductivity elasticity is modest, but Figure 2 shows that the response can still be strongly nonlinear over the full range $k_w/k_s \in [0.1,1]$. The largest practical uncertainty arises from the imposed surface superheat and the initial thermal state, which are accounted for through $Ste$ and $\phi$. Accurate surface-temperature characterization should therefore be a priority when applying the solution to field sites.

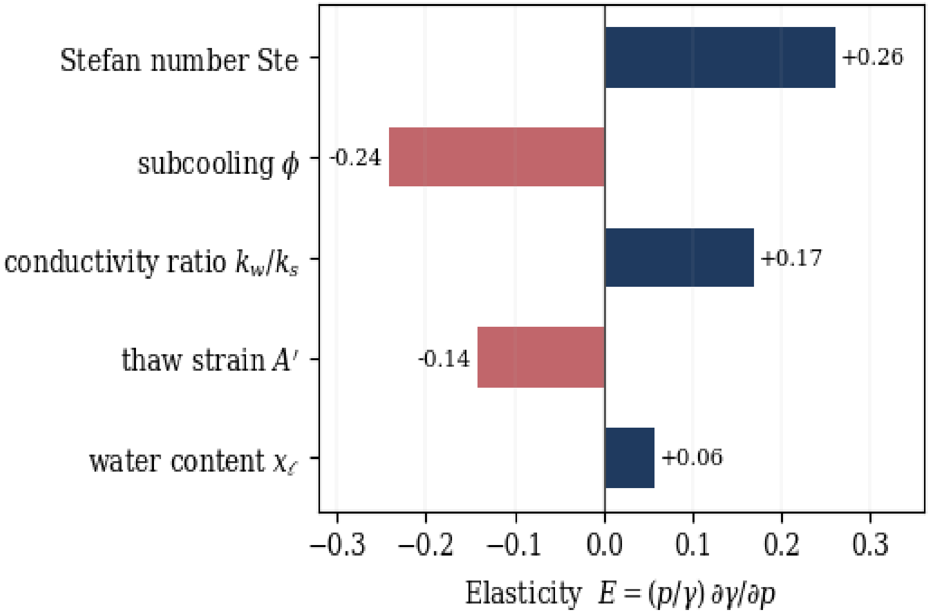

**Figure 4.** Dimensionless sensitivity elasticities $E = (p/\gamma)\,\partial\gamma/\partial p$ at the baseline case. Positive (blue) inputs increase the thaw parameter, negative (red) decrease it. All $|E| < 1$.

## 3.3 Numerical model and validation

We use an independent enthalpy/apparent heat capacity finite-difference model (Voller & Cross, 1981) to verify the exact solution and handle time-varying forcing. In the model, latent heat is released over a narrow temperature interval through an apparent volumetric heat capacity. Thermal conductivity and heat capacity vary smoothly between frozen and thawed values as a function of the liquid fraction. Time integration uses a backward-Euler scheme with a tridiagonal solver, and temperature-dependent properties are updated by Picard iteration.

Under a constant surface temperature, the numerical model should reproduce the exact thaw depth, $X_3 = 2\gamma\sqrt{\alpha_2 t}$. Figure 5(a) confirms this, for representative saturated-soil properties ($k_2 = 1.5\,W.m^{-1.K^{-1}}$, $k_3 = 2.2\,W.m^{-1.K^{-1}}$, volumetric water content 0.35, $T_s = 5\,°C$, $T_0 = -4\,°C$, giving Ste $= 0.11$, $\phi = 0.8$), the numerical and analytical thaw depths agree with a mean error of 2.5%. Refining the grid and narrowing the phase-change interval reduces the error to about 1.4%, as expected. This comparison provides a useful implementation check and supports the use of the numerical model for seasonal forcing, where no exact similarity solution is available.

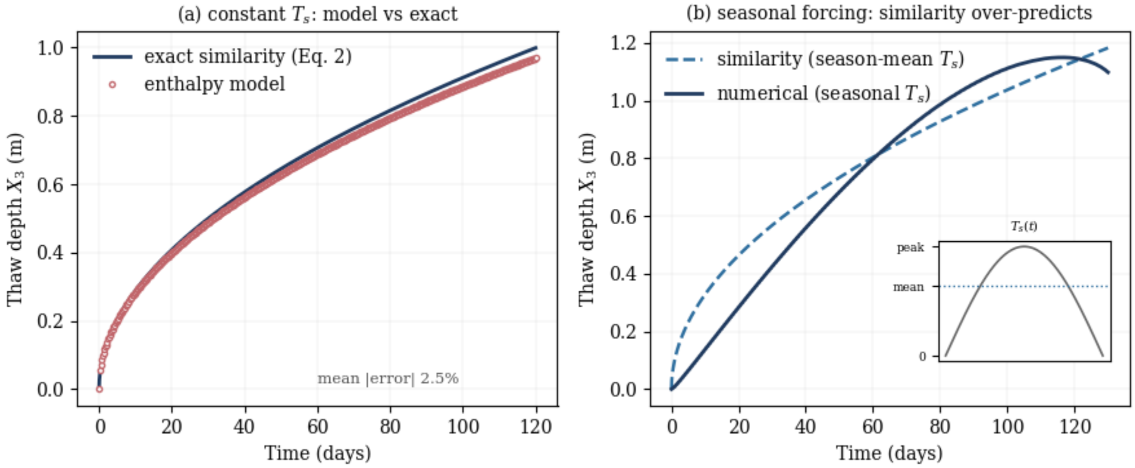

**Figure 5.** (a) Cross-validation under a constant surface temperature: the enthalpy model (circles) reproduces the exact similarity solution (line) with a mean error of 2.5%. (b) Under seasonal forcing, represented by a half-sine surface temperature with a peak of 10 °C, the similarity solution evaluated at the season-mean temperature (dashed) advances the thaw trajectory relative to the transient numerical solution (solid). For active-layer-thickness estimates, the relevant metric is the seasonal maximum thaw-front depth rather than the instantaneous front position.

# 4. Active-layer thaw and subsidence at a Svalbard site

## 4.1 Study site and forcing

We demonstrate the approach using the Calypsostranda site in Bellsund, SW Spitsbergen, Svalbard, as an illustrative field-scale case. The Calypsostranda transect in Bellsund is CALM site P1 and has active-layer and ground-temperature records extending back to the 1980s (Brown et al., 2000; Marsz et al., 2013). The site consists of fine-textured, ice-bearing sediments and is well-suited for testing a thaw-consolidation model.

Three features make the site useful for this purpose. First, Svalbard contains some of the warmest permafrost in the Nordic region. Near the coast, ground temperatures are close to 0 °C, so latent heat strongly controls the thermal response (Christiansen et al., 2010). Second, the fine-grained, ice-bearing active layer is the type of material in which thaw consolidation matters, and a zero-strain Stefan model is least appropriate. Soil moisture is also known to influence year-to-year active-layer thickness in Svalbard (Schuh et al., 2017). Third, the observational record is long enough to provide a meaningful comparison. At Calypsostranda, late-summer active-layer thickness averaged about 1.18 m over 1986–2009 and reached 1.2–1.7 m in warm years (Marsz et al., 2013). These values fall within the broader context of circum-Arctic active-layer thickening reported since 2000 (Smith et al., 2022).

The thermal forcing used here is deliberately simple. We prescribe a representative thaw season as a half-sine surface temperature with a peak of 10 °C and a duration of 130 days, giving a season-mean temperature of 6.4 °C. The initial ground temperature is set to -4 °C, and the soil properties are the saturated fine-soil values used in Section 3.3. These are representative rather than site-calibrated values. These values are broadly consistent with the reported warm-season climate of the Bellsund/Calypsostranda area, where mean summer air temperature at Calypsobyen is about 5 °C, while the conversion from air to ground-surface temperature is represented here using a simple thawing *n*-factor approach (Marsz et al., 2013; Etzelmüller et al., 2011; Kurylyk et al., 2014). The aim is not to produce a fully tuned simulation, but to test whether the thaw-consolidation solution gives realistic active-layer and settlement magnitudes under plausible Arctic conditions. The resulting Stefan number $Ste \approx 0.1$ places the problem in the small-Stefan regime typical of thawing permafrost. A more detailed site study would replace the idealised half-sine forcing with recorded surface temperatures from the Calypsostranda (Calypsobyen) station, converted from air temperature using a site-specific n-factor, and would use measured local soil properties.

## 4.2 Accuracy of the similarity solution under seasonal forcing

Figure 5b compares two thaw trajectories. The first is the transient numerical solution driven by the half-sine seasonal temperature. The second is the similarity solution evaluated using the season-mean surface temperature, which is the most straightforward way to apply the closed-form formula to a thaw season. Both cases have the same total thawing degree-days, about 828 °C·d. The difference between them, therefore, comes from the timing of heat delivery, not from the total amount of heat supplied at the surface.

The difference is clear. The similarity solution follows a $\sqrt{t}$ trajectory from the start of the season. In contrast, the transient solution thaws slowly early in the season, when surface temperatures are still low, and accelerates toward midsummer. As a result, the constant-temperature approximation over-predicts mid-season thaw depth by about 13%, reaches 0.5 m roughly twelve days too early, and over-predicts end-of-season active-layer thickness by about 8%. The reason is simple: a step change to the season-mean temperature front-loads heat, while real seasonal forcing delivers much of the heat later.

This timing error matters. Many active-layer processes depend not only on the maximum thaw depth, but also on when the thaw front reaches a given depth. The onset of supra-permafrost flow, seasonal runoff partitioning, microbial activity at depth, and ground trafficability are all tied to the thaw trajectory (Walvoord and Kurylyk, 2016). A model that places the thaw front almost two weeks too early will bias these process timings. The end-of-season error is smaller and may be acceptable for rapid estimates of maximum active-layer thickness. Thus, the similarity solution is useful for end-of-season calculations, but a transient model is preferable when the timing of thaw propagation is important.

## 4.3 Predicted thaw and settlement

Figure 6 shows the predicted thaw-front trajectory and the associated kinematic settlement estimate for the representative Svalbard thaw season. The model reaches an end-of-season thaw depth of about 1.1 m. This is close to the reported long-term Calypsostranda mean of 1.18 m and slightly below the 1.2–1.7 m range observed in warm years (Marsz et al., 2013). Because the thermal properties, water content, and forcing were prescribed independently rather than tuned to match the observed active-layer thickness, the comparison suggests that the thaw-consolidation solution captures the right first-order behaviour in this latent-heat-dominated setting. A stronger test would require measured soil properties and recorded surface forcing.

Using the instantaneous thaw-front depth $X_3(t)$, the associated kinematic settlement estimate is $S(t) = A' X_3(t)$. Because this illustrative case uses a small thaw strain ($A'$=0.05), the settlement curve is interpreted here as a drained kinematic estimate rather than as a cumulative settlement prediction for a retained excess-water-layer case. With this thaw strain, which is appropriate for fine-textured, moderately ice-rich material, the predicted settlement estimate reaches about 5.5 cm by the end of the thaw season. This magnitude is consistent with seasonal thaw subsidence observed over wet, fine-grained permafrost soils, which is typically a few centimetres and larger than the sub-2 cm movement of dry, coarse ridges (Shiklomanov et al., 2013; Streletskiy et al., 2017, 2025).

The calculation illustrates the main value of Lunardini's solution: thaw depth and settlement are linked in one transparent expression. Zero-strain Stefan solutions can predict thaw depth, but not surface lowering. Here, the same thaw parameter controls both. The settlement estimate depends linearly on the prescribed thaw strain ($A'$), so a site-specific value derived from local ice content would improve the subsidence prediction without changing the thermal calculation. This is particularly useful because seasonal and interannual thaw subsidence are now being mapped across permafrost regions using satellite observations (Liu et al., 2010). A simple analytical connection between surface forcing, thaw depth, and settlement can help interpret those observations and provide quick checks on more complex models.

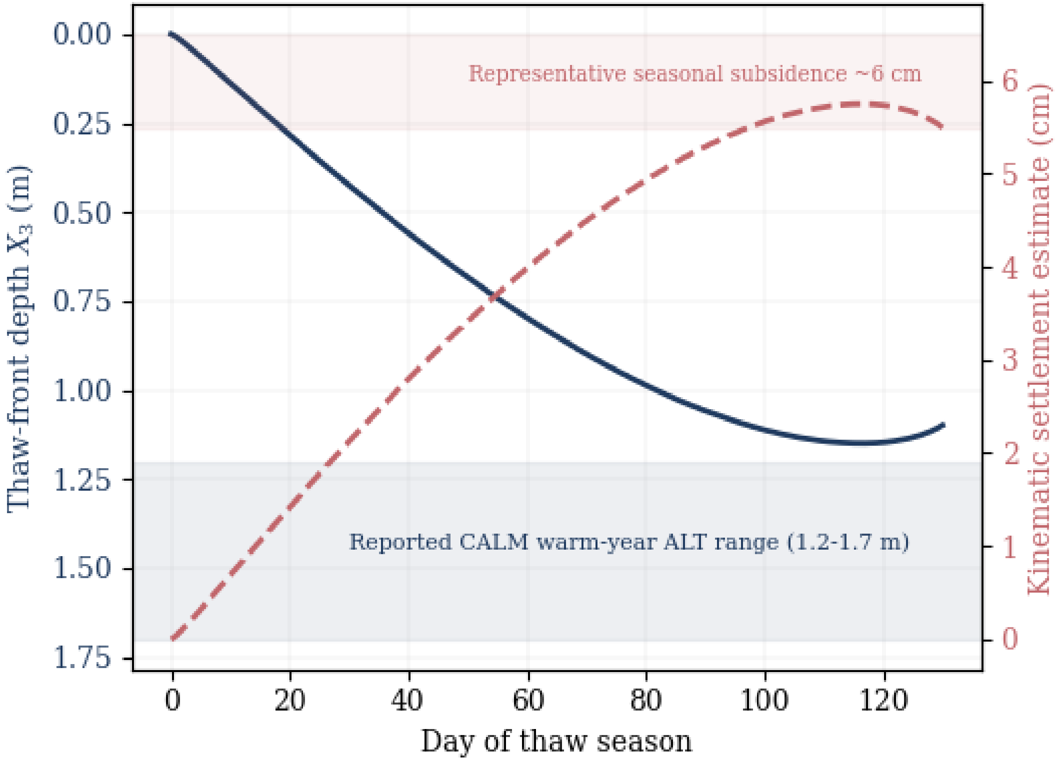

**Figure 6.** Predicted instantaneous thaw-front depth $X_3(t)$ (left axis, inverted) and the associated kinematic settlement estimate $S(t) = A'X_3(t)$ (right axis) over the representative thaw season at the Calypsostranda CALM site (Bellsund). The shaded band for thaw depth marks the reported warm-year active-layer-thickness range of approximately 1.2–1.7 m. In contrast, the settlement band indicates a representative seasonal subsidence scale of about 6 cm.

## 5. Discussion

The results make Lunardini's exact solution more accessible for practical use. The small- and large-Stefan approximations remove the need for root-finding in the most important limiting cases. The small-Stefan approximation is especially useful for permafrost, where latent heat keeps $Ste$ low, and thaw is slow. The sensitivity analysis shows that the thaw parameter is not highly fragile: near the baseline case, all elasticities are below 1. In practice, moderate input errors do not lead to larger relative errors in predicted thaw depth. The largest sensitivities are associated with surface thermal forcing, which means that careful treatment of surface temperature is more important than small refinements to some soil parameters.

The transient forcing experiment gives the main caution. A season-mean surface temperature may preserve the correct thawing degree-days, but it does not preserve the timing of heat delivery. As a result, the similarity solution thaws too quickly early in the season and reaches intermediate depths too soon. The final active-layer thickness is only modestly over-predicted, by about 8%, but the thaw trajectory is shifted forward by nearly two weeks. This distinction is important. For rapid estimates of end-of-season active-layer thickness, the closed-form solution is likely adequate. For questions involving runoff timing, microbial activation, trafficability, or seasonal deformation history, a transient model should be used.

The Svalbard application shows that the method gives realistic first-order predictions under plausible Arctic conditions. With representative forcing and independently specified soil properties, it predicts an active-layer thickness close to the long-term Calypsostranda mean and a drained kinematic settlement estimate of about 5.5 cm. This should not be read as a fully calibrated site validation. Rather, it shows that the thaw-consolidation physics retained in the analytical solution is sufficient to reproduce the correct scale of both thaw depth and surface lowering. That is a useful result, because it places the solution between simple zero-strain Stefan estimates and fully coupled THM simulations.

The limitations are also clear. The solution is one-dimensional, saturated, and based on a sharp thaw front. It uses a prescribed thaw strain and does not solve for pore-pressure dissipation or stress-dependent deformation. It also does not represent unfrozen-water retention, salinity, vapour flow, lateral water movement, snow insulation, vegetation effects, or soil layering unless these are added through extensions or effective parameters. Fully coupled thermo-hydro-mechanical models remain necessary when these processes control the problem (Huang and Rudolph, 2021). The analytical solution is therefore best viewed as a fast end-member model, a screening tool, and a benchmark for more complex simulations, rather than as a replacement for them.

Several extensions would make the approach more useful. The first is straightforward: use recorded surface-temperature series and measured soil properties at the Calypsostranda site instead of idealized forcing and representative parameters. The second is to include a finite freezing interval or unfrozen-water curve more directly, rather than representing phase change only through the numerical enthalpy window. The third is to link the thaw strain ($A'$) to the consolidation theory so that pore pressure, ice content, and settlement evolve together. These additions would move the method closer to coupled THM models while preserving the clarity and speed that make the analytical solution valuable.

## 6. Conclusions

In this study, we revisited the exact thaw-consolidation solution of Lunardini (1987) and developed it into a more practical tool for active-layer and thaw-subsidence prediction. The main results are as follows.

(1) Small- and large-Stefan-number approximations provide simple estimates of the thaw parameter without numerical root-finding. The small-Stefan approximation is accurate to about 2% in the permafrost-relevant regime, while the large-Stefan approximation is accurate to about 1.3% for high superheat.

(2) The sensitivity analysis shows that the thaw parameter responds sub-proportionally to all major inputs near the baseline case. The largest practical uncertainty arises from the imposed surface superheat and the

initial thermal state, which together enter through the Stefan number and the subcooling parameter.

(3) An independent enthalpy finite-difference model reproduces the exact solution with a mean error of 2.5% under constant surface temperature, providing a useful check on the analytical implementation and a tool for transient forcing.

(4) Seasonal forcing introduces a timing bias that the similarity solution cannot capture. Using a season-mean surface temperature over-predicts end-of-season active-layer thickness by about 8% and places the thaw front roughly two weeks too early during the season.

(5) In an illustrative Svalbard application with representative forcing and independently specified fine-soil properties, the model predicts an active-layer thickness of the correct order and a drained kinematic thaw-settlement estimate of about 5.5 cm.

Overall, the solution provides a useful bridge between simple Stefan-type estimates and full transient THM models. It is best suited for rapid end-of-season active-layer estimates, thaw-subsidence screening, and model benchmarking. When the timing of thaw propagation, transient hydrological response, or coupled hydro-mechanical feedbacks is important, a transient numerical model remains necessary.

## Code and data availability

The solver for Equation (2), the asymptotic and sensitivity routines, and the enthalpy finite-difference model are provided as documented Python scripts in the accompanying repository (or Supplementary Materials). Active-layer thickness and ground-temperature records for the study site are distributed through the CALM programme (Brown et al., 2000).

## Nomenclature

| | | | |
|---|---|---|---|
| $A = A' + \rho_{iw} - 1$ | | $T_f, T_0, T_s$ | fusion, initial, surface temperature |
| $A'$ | soil thaw strain | $X_3$ | thaw depth (active-layer thickness) |
| $c$, $C$ | specific / volumetric heat capacity | $x_\ell$ | volumetric water content |
| $E_p$ | elasticity $(p/\gamma)\ \partial\gamma/\ \partial p$ | $\alpha$ | thermal diffusivity |
| $k$ | thermal conductivity | $\gamma$ | thaw parameter |
| $K$ | $= (\rho_w c_w/\rho_2 c_2)\, A$ | $\rho$ | density; $\rho_{iw} = \rho_i/\rho_w$ |
| $L_\ell$ | latent heat of fusion | $\phi$ | $= (T_f - T_0)/(T_s - T_f)$, subcooling |
| $S$ | thaw settlement | *subscripts* | |
| Ste | $(c_2/L_\ell)(T_s - T_f)$, Stefan number | $i, s, w$ | ice, soil solids, water |
| $t$ | time | 1, 2, 3 | water, thawed, frozen regions |

## References

Biskaborn, B. K., S. L. Smith, J. Noetzli, et al. (2019) Permafrost is warming at a global scale. *Nature Communications*, 10, 264. https://doi.org/10.1038/s41467-018-08240-4

Brown, J., K. M. Hinkel, and F. E. Nelson (2000) The Circumpolar Active Layer Monitoring (CALM) program: research designs and initial results. *Polar Geography*, 24(3), 166–258. https://doi.org/10.1080/10889370009377698

Christiansen, H. H., B. Etzelmüller, K. Isaksen, et al. (2010) The thermal state of permafrost in the Nordic area during the International Polar Year 2007–2009. *Permafrost and Periglacial Processes*, 21, 156–181. https://doi.org/10.1002/ppp.687

Etzelmüller, B., Schuler, T. V., Isaksen, K., Christiansen, H. H., Farbrot, H., and Benestad, R. (2011). Modeling the temperature evolution of Svalbard permafrost during the 20th and 21st century. The Cryosphere, 5, 67–79. https://doi.org/10.5194/tc-5-67-2011

Hjort, J., D. Streletskiy, G. Doré, et al. (2022) Impacts of permafrost degradation on infrastructure. *Nature Reviews Earth & Environment*, 3, 24–38. https://doi.org/10.1038/s43017-021-00247-8

Huang, X., and D. L. Rudolph (2021) Coupled model for water, vapour, heat, stress and strain fields in variably saturated freezing soils. *Advances in Water Resources*, 154, 103945. https://doi.org/10.1016/j.advwatres.2021.103945

Huang, X., and D. L. Rudolph (2022) A hybrid analytical–numerical technique for solving soil temperature during the freezing process. *Advances in Water Resources*, 162, 104163. https://doi.org/10.1016/j.advwatres.2022.104163

Huang, X., D. L. Rudolph, and B. Glass (2022) A coupled thermal–hydraulic–mechanical approach to modeling the impact of roadbed frost loading on water main failure. *Water Resources Research*, 58(3), e2021WR030933. https://doi.org/10.1029/2021WR030933

Kurylyk, B. L., J. M. McKenzie, K. T. B. MacQuarrie, and C. I. Voss (2014) Analytical solutions for benchmarking cold regions subsurface water flow and energy transport models: one-dimensional soil thaw with conduction and advection. *Advances in Water Resources*, 70, 172–184. https://doi.org/10.1016/j.advwatres.2014.05.005

Kurylyk, B. L. (2019). Engineering challenges of warming. *Nature Climate Change*, 9(11), 807-808. https://doi.org/10.1038/s41558-019-0612-8

Liu, L., T. Zhang, and J. Wahr (2010) InSAR measurements of surface deformation over permafrost on the North Slope of Alaska. *Journal of Geophysical Research*, 115, F03023.

Lunardini, V. J. (1981) *Heat Transfer in Cold Climates*. Van Nostrand Reinhold, New York.

Lunardini, V. J. (1983). Freezing and Thawing: Heat Balance Integral Approximations. *Journal of Energy Resources Technology*, 105(1): 30-37. https://doi.org/10.1115/1.3230872

Lunardini, V. J. (1987) Exact solution for melting of frozen soil with thaw consolidation. U.S. Army Cold Regions Research and Engineering Laboratory (CRREL), 97–102.

Lunardini, V. J., and R. Varotta (1981) Approximate solution to the Neumann problem for soil systems. *Journal of Energy Resources Technology*, 103(1), 76–81. https://doi.org/10.1115/1.3230817

Lunardini, V. J. (1991). *Heat transfer with freezing and thawing* (Vol. 65). Elsevier.

Marsz, A. A., Styszyńska, A., Pękala, K., & Repelewska ‐ Pękalowa, J. (2013). Influence of meteorological elements on changes in active‐layer thickness in the Bellsund region, Svalbard. *Permafrost and Periglacial Processes*, 24(4), 304-312. https://doi.org/10.1002/ppp.1790

Morgenstern, N. R., and J. F. Nixon (1971) One-dimensional consolidation of thawing soils. *Canadian Geotechnical Journal*, 8, 558–565. https://doi.org/10.1139/t71-057

Nixon, J. F. (1975) The role of convective heat transport in the thawing of frozen soils. *Canadian Geotechnical Journal*, 12, 425–429. https://doi.org/10.1139/t75-049

Obu, J., S. Westermann, A. Bartsch, et al. (2019) Northern Hemisphere permafrost map based on TTOP modelling for 2000–2016 at 1 km$^2$ scale. *Earth-Science Reviews*, 193, 299–316. https://doi.org/10.1016/j.earscirev.2019.04.023

Peng, X., T. Zhang, O. W. Frauenfeld, et al. (2023) Active layer thickness and permafrost area projections for the 21st century. *Earth's Future*, 11, e2023EF003573. https://doi.org/10.1029/2023EF003573

Ran, Y., Cheng, G., Dong, Y., Hjort, J., Lovecraft, A. L., Kang, S., ... & Li, X. (2022). Permafrost degradation increases risk and large future costs of infrastructure on the Third Pole. *Communications Earth & Environment*, 3(1), 238. https://doi.org/10.1038/s43247-022-00568-6

Rantanen, M., A. Yu. Karpechko, A. Lipponen, et al. (2022) The Arctic has warmed nearly four times faster than the globe since 1979. *Communications Earth & Environment*, 3, 168. https://doi.org/10.1038/s43247-022-00498-3

Schuh, C., A. Frampton, and H. H. Christiansen (2017) Soil moisture redistribution and its effect on inter-annual active layer temperature and thickness variations in a dry loess terrace in Adventdalen, Svalbard. *The Cryosphere*, 11(1), 635–651. https://doi.org/10.5194/tc-11-635-2017

Shiklomanov, N. I., D. A. Streletskiy, J. D. Little, and F. E. Nelson (2013) Isotropic thaw subsidence in undisturbed permafrost landscapes. *Geophysical Research Letters*, 40(24), 6356–6361. https://doi.org/10.1002/2013GL058295

Smith, S. L., H. B. O'Neill, K. Isaksen, J. Noetzli, and V. E. Romanovsky (2022) The changing thermal state of permafrost. *Nature Reviews Earth & Environment*, 3, 10–23. https://doi.org/10.1038/s43017-021-00240-1

Streletskiy, D. A., N. I. Shiklomanov, J. D. Little, et al. (2017) Thaw subsidence in undisturbed tundra landscapes, Barrow, Alaska, 1962–2015. *Permafrost and Periglacial Processes*, 28(3), 566–572. https://doi.org/10.1002/ppp.1918

Streletskiy, D. A., A. Maslakov, G. Grosse, et al. (2025) Thawing permafrost is subsiding in the Northern Hemisphere-review and perspectives. *Environmental Research Letters*, 20, 013006. https://doi.org/10.1088/1748-9326/ada2ff

Turetsky, M. R., B. W. Abbott, M. C. Jones, et al. (2020) Carbon release through abrupt permafrost thaw. *Nature Geoscience*, 13, 138–143. https://doi.org/10.1038/s41561-019-0526-0

Voller, V., and Cross, M. (1981). Accurate solutions of moving boundary problems using the enthalpy method. International journal of heat and mass transfer, 24(3), 545-556.

Walvoord, M. A., and B. L. Kurylyk (2016) Hydrologic impacts of thawing permafrost—a review. *Vadose Zone Journal*, 15(6), 1–20. https://doi.org/10.2136/vzj2016.01.0010

Xiang, H., and D. L. Rudolph (2023) Numerical study of coupled water and vapor flow, heat transfer, and solute transport in variably-saturated deformable soil during freeze–thaw cycles. *Water Resources Research*, 59(10), e2022WR032146. https://doi.org/10.1029/2022WR032146

Xie, C., and W. A. Gough (2013) A simple thaw–freeze algorithm for a multi-layered soil using the Stefan equation. *Permafrost and Periglacial Processes*, 24, 252–260. https://doi.org/10.1002/ppp.1770